Evolution-Based Design of an Injectable Hydrogel

*Iris M. Geisler and Joel P. Schneider**

A new class of simple, linear, amphiphilic peptides are developed that have the ability to undergo triggered self-assembly into self-supporting hydrogels. Under non-gelling aqueous conditions, these peptides exist in a random coil conformation and peptide solutions have the viscosity of water. On the addition of a buffered saline solution, the peptides assemble into a β-sheet rich network of fibrils, ultimately leading to hydrogelation. A family of nine peptides is prepared to study the influence of peptide length and amino acid composition on the rate of self-assembly and hydrogel material properties. The amino acid composition is modulated by varying residue hydrophobicity and hydrophilicity on the two opposing faces of the amphiphile. The conformation of peptides in their soluble and gel state is studied by circular dichroism (CD), while the resultant material properties of their gels is investigated using oscillatory sheer rheology. One weight percent gels formed under physiological conditions have storage modulus (G') values that vary from ≈20 to ≈800 Pa, with sequence length and hydrophobic character playing a dominant roll in defining hydrogel rigidity. Based on the structural and functional data provided by the nine-peptide family members, an optimal sequence, namely LK13, is evolved. LK13 (LKLKLKLKLKLKL-NH_2) undergoes triggered self-assembly, affording the most rigid gel of those studied (G'=797 ± 105). It displays shear thin-recovery behavior, allowing its delivery by syringe and is cytocompatibile as assessed with murine C3H10t1/2 mesenchymal stem cells.

1. Introduction

Hydrogels are an attractive biomaterial for use in tissue engineering and drug delivery that have the ability to retain a substantial amount of water while maintaining a distinct three-dimensional structure.[1] The earliest uses of hydrogels reach back to 1960, when hydrogel networks were first applied in the fabrication of soft contact lenses.[2] Since then, interest in hydrogels has grown due to their potential use in a myriad of applications and research within this area continues to be vibrant. Hydrogels can be constructed from almost any water-soluble polymer capable of forming a cross-linked network through either covalent or physical interactions. Historically, many hydrogels were prepared synthetically from high molecular weight polymers derived from ethylene oxide, vinyl alcohol, and acrylic acid derivatives or from natural products such as collagen, gelatin, fibrin, and various polysaccharide derivatives.[3] More recently, smaller entities, such as self-assembling peptides, have been utilized in the construction of hydrogels.[4–6] The design of hydrogels using peptides are of particular interest since hydrogelation is primarily driven by physical interactions, such as hydrogen bonding and hydrophobic association, eliminating the need for chemical cross-linking.

Much attention has been given to the development of injectable hydrogels to facilitate localized drug delivery and cell therapy through simple injection.[7,8] Injectable gels or gel-forming materials have several advantages over pre-formed implantations, including their minimally invasive introduction in vivo and ability to optimally fill nearly any cavity or defect. Hence, injectable hydrogels that can be used to homogeneously encapsulate cells and/or various therapeutic cargoes make them excellent candidates for tissue engineering and drug delivery applications. Injectable systems that afford gels that remain localized at the area of injection and avoid leakage to neighboring tissues are most effective. Many of the reported injectable gels are actually liquids that once injected undergo a sol–gel phase transition or are chemically polymerized in situ.[7] The various triggers that have been utilized to induce an in vivo sol–gel transition include salt,[9] temperature,[10] enzymes,[11] and photoinitiated polymerization.[12] Despite its many advantages, one major draw back of in situ hydrogelation is the high potential for unwanted leakage of the gel precursor. This is especially problematic if the rate of the sol–gel phase transition is slow.

One approach to circumvent this problem is to use pre-formed solid-gels that can be syringe delivered. For example, Schneider and Pochan et al. have developed an injectable gel prepared from self-assembling β-hairpin peptides. These gels shear thin and flow under applied stress, but recover their solid properties on removal of the applied stress, allowing their delivery from a simple syringe.[5,13] Other shear-thinning and self-healing gels composed of peptides have also been reported.[14]

Herein, we present the design of a class of simple, short, linear, amphiphilic peptides that have the ability to undergo

Dr. I. M. Geisler, Prof. J. Schneider
National Cancer Institute
National Institute of Health
Frederick, MD 21702, USA
E-mail: Joel.Schneider@nih.gov

DOI: 10.1002/adfm.201102330

triggered self-assembly into β-sheet rich fibrils that constitute a self-supporting gel with shear-thinning and self-healing properties. As will be shown, self-assembly leading to gelation is triggered by simply adjusting the ionic strength of a solution of unfolded peptide. A family of nine peptides was prepared to study the influence of sequence length and hydrophobic as well as hydrophilic content on hydrogelation. From these results, an optimized sequence was evolved that is capable of triggered hydrogelation affording a shear-thin deliverable material that is also cytocompatible.

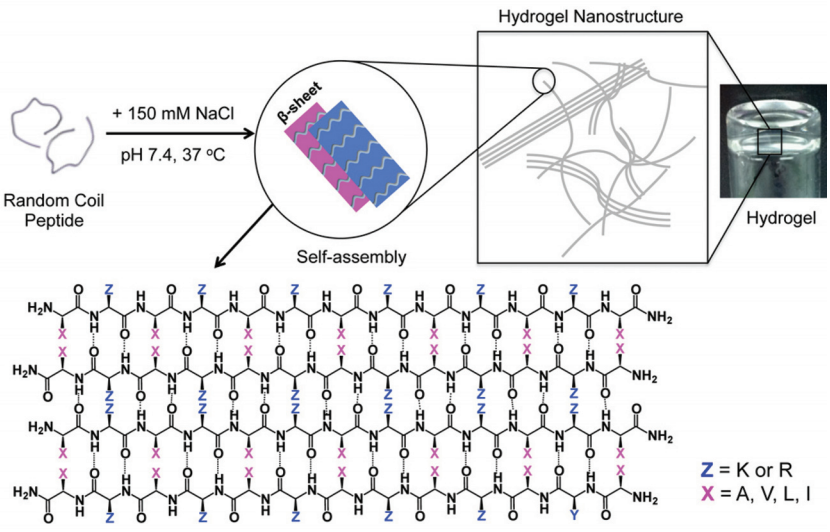

Figure 1. Proposed model of peptide self-assembly into fibrils that constitute the hydrogel. Each fibril is composed of a bilayer of hydrogen-bonded β-strands. H-bond formation occurs along the long-axis of a given fibril. Blue lettering and shading depicts hydrophilic amino acid side chains; hydrophobic side chains are shown in pink.

2. Results and Discussion

2.1. Peptide Design

Peptide amphiphilicity, the facially opposing display of hydrophilic and hydrophobic amino acid side chains is commonly employed in the design of self-assembling peptides. In aqueous solution, the association of hydrophobic side chains typically provides the driving force for self-assembly. The formation of polar interactions such as hydrogen bonds and salt bridges provide structural specificity. For assemblies rich in β-sheet secondary structure, amphiphilicity is conferred to the peptide by simply alternating hydrophobic and hydrophilic amino acids along a linear sequence (e.g., $(AB)_n$).

The parent peptide for this study, VK11 (VKVKVKVKVKV-NH_2), is an 11 amino acid repeat of valine and lysine residues. Its simple design was based on the early report of Orgel that showed that a poly(Val-Lys) sequence of about 50 residues could undergo an ionic-strength dependent random coil to β-sheet conformational change that was coupled to self-assembly.[15] In addition, the Val-Lys repeating unit is a common element in β-sheet peptidomimetic design[16] and in the design of self-assembling β-hairpins reported by our group. The β-branched side chain of valine confers a high propensity for this residue to adopt dihedral angles consistent with β-structure. Lysine, although often defined as a hydrophilic residue, has a relatively hydrophobic alkyl chain that is decorated with a positive point charge at its end. Alternating these two residues affords a relatively hydrophobic amphiphilic sequence with a high propensity to adopt β-sheet secondary structure and a large penchant for self-assembly.

VK11 is designed such that at physiological pH, its lysine side-chains are protonated rendering the peptide soluble in an aqueous solution of low ionic strength. However, when the ionic strength is increased via the addition of NaCl, screening of the lysine-borne charge should allow the peptide to self-assemble. Self-assembly should then be driven mainly by intermolecular hydrophobic contacts made between valine side chains. In addition, hydrophobic contacts made between the methylene groups of neighboring lysine side chains may also help drive self-assembly. The formation of intermolecular hydrogen bonds between amide bond H-bond donors and acceptors should help dictate the overall nanoscale morphology of the self-assembled structure, in this case, β-sheet rich fibrils. We envision that each fibril in the network is composed of a bilayer of extended β-sheets, where each sheet contains individual β-strand peptides that intermolecularly H-bond along the long axis of a given fibril. Bilayer formation is driven by the hydrophobic collapse of the hydrophobic faces (shown in pink in **Figure 1**) of the two β-sheets that define the bilayer. As will be shown, fibrils can assemble further to form laminated structures. Whether or not laminates are formed depends on the exact sequence of the peptide. At any rate, the simple entanglement of the resulting fibrils and/or laminates leads to hydrogelation (Figure 1).

The effect of sequence length on gelation was investigated via the preparation of four additional peptides. Two shorter peptides, namely VK9 and VK10, and two longer peptides, VK12 and VK13, which vary in residue number, but contain the same type of residues in their sequences (**Table 1**). Along with VK11, this family spans 9 to 13 residues. As will be shown, a sequence

Table 1. Name and peptide sequences. The N-terminus is the free amine and the C-terminus is the carboxyamide.

Peptide Name	Sequence
VK9	VKVKVKVKV-NH_2
VK10	VKVKVKVKVK-NH_2
VK11	VKVKVKVKVKV-NH_2
VK12	VKVKVKVKVKVK-NH_2
VK13	VKVKVKVKVKVKV-NH_2
AK13	AKAKAKAKAKAKA-NH_2
IK13	IKIKIKIKIKIKI-NH_2
LK13	LKLKLKLKLKLKL-NH_2
VR13	VRVRVRVRVRVRV-NH_2

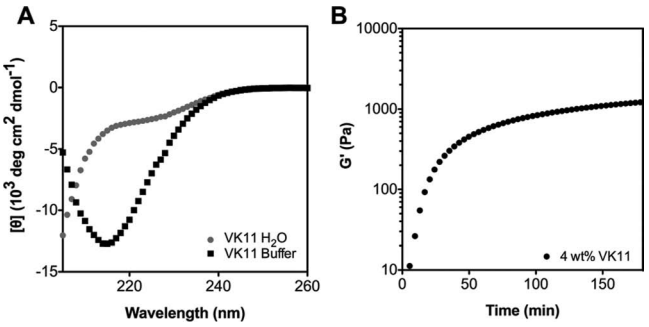

Figure 2. CD spectroscopy and oscillatory rheology of the VK11 hydrogel. A) CD spectra of 2 wt% VK11 in water (●) and pH 7.4 50 mM BTP and 150 mM NaCl buffer (■) at 35 °C. B) Dynamic time sweep of 4 wt% VK11 in pH 7.4 50 mM BTP and 150 mM NaCl buffer at 37 °C.

length of 13 residues, e.g., VK13, proved optimal. The influence of altering the identity of the hydrophobic residues was probed with three additional peptides where all the valines of VK13 were replaced with either alanine, leucine, or isoleucine. Finally, one additional peptide was prepared in which arginine was used to replace all the lysine residues of the amphiphile to study the importance of the identity of the hydrophilic residue.

2.2. Hydrogelation of the Parent Peptide VK11

VK11 is designed to self-assemble into a β-sheet rich network of fibrils when solution conditions permit. Circular dichroism (CD) studies were performed to assess the change in peptide conformation upon self-assembly, when saline buffer is added to an aqueous solution of VK11. **Figure 2**A shows wavelength-dependent CD spectra of 2 wt% VK11 dissolved in water alone and after the addition of saline buffer. When VK11 is dissolved in water, it displays a spectrum consistent with a random coil conformation, indicating that the peptide has not undergone self-assembly. However, when the ionic strength of the VK11 solution is increased by adding a concentrated buffered (pH 7.4) saline solution (100 mM bis-trispropane (BTP), 300 mM NaCl) to an equal amount of aqueous peptide (resulting in 150 mM NaCl, 2 wt% peptide), there was a clear change in the spectrum, which displayed a minimum at 216 nm and a spectral shape consistent with β-sheet secondary structure. This suggests that the addition of NaCl results in the screening of the lysine charge, permitting self-assembly to take place, resulting in assemblies rich in β-sheet structure. This change in CD signal from random coil to β-sheet, was accompanied by hydrogelation directly in the CD cell.

Hydrogelation was further studied by oscillatory rheology. Figure 2B shows the storage modulus (G') measured at 37 °C as a function of time over a 3 h period immediately after the addition of BTP saline buffer to an aqueous solution of peptide. A 4 wt% solution of VK11 undergoes immediate gelation when triggered. The rigidity of the gel increases to ≈500 Pa at 60 min and then continues to slowly rigidify over time (≈1250 Pa). The rheological time sweep measurements were performed at a frequency of 6 rad $s^{-1}$and 0.2% strain. Dynamic frequency (0.1–100 rad s^{-1} at 0.2% strain) and dynamic strain (0.1–1000% at 6 rad s^{-1}) sweep measurements were performed to verify that the time-sweep measurements were within the linear viscoelastic regime (see Supporting Information). While rheology was performed at a peptide concentration of 4 wt%, half this concentration was used for the CD experiments to stay within the workable detection range of the instrument.

2.3. Influence of Sequence Length

In order to investigate the influence of peptide sequence length on the self-assembly kinetics and resultant material properties, four additional peptides were prepared that are either truncated by one (VK10) or two (VK9) amino acid residues or elongated by one (VK12) or two (VK13) amino residues with respect to VK11 (Table 1). Their rates of hydrogelation and the mechanical rigidity of their gels were assessed by oscillatory shear rheology. **Figure 3**A shows dynamic time sweep data for each gel at a peptide concentration of 4 wt%. The differences in hydrogelation kinetics were found to vary noticeably between the different length peptides. VK13 displayed the fastest rate of gelation, forming a strong hydrogel of >2000 Pa after less than 20 min that continued to increase in rigidity over a period of 3 h. In comparison, VK9 and VK11 formed gels at much slower rates. Interestingly, no appreciable hydrogelation was observed in case of VK10 and VK12. The differences in the final storage moduli of the peptide gels are shown in Figure 3B. VK13 forms the most rigid gel with a G' of 6136 ± 254 after 3 h. The shorter peptides VK9 and VK11 formed less rigid gels having G' values of 1542 ± 143 and 1267 ± 48, respectively, while storage moduli of <30 Pa were observed for the VK10 and VK12 gels. For all the peptides studied, the time-sweep data shows that the onset of gelation, as monitored by the increase of G' as a function of time, occurs over two distinct time regimes. A fast burst in G', which represent peptide self-assembly and the formation of physical crosslinks, followed by a slower phase. During the

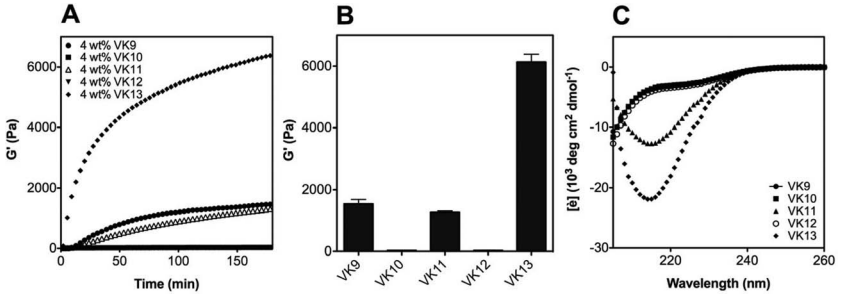

Figure 3. Rheological measurements and CD spectroscopy of VK9-13 hydrogels. A) Time sweeps of 4 wt% VK9–13 peptide hydrogels after the addition of 100 mM BTP and 300 mM NaCl pH 7.4 to an aqueous solution of each peptide. B) Comparison of storage moduli of VK9–13 hydrogels at t = 3 h. C) CD spectra of 2 wt% VK9-13 hydrogels in BTP buffer at 35 °C.

slower curing phase, the value of G' slowly increases and never reaches a true equilibrium within the time frame of the experiment. However, since the increase in G' realized during this phase is minimal, we treat this regime as a pseudo-equilibrium and extract values of G' for each of the peptide gels at a common time point so that comparisons can be made. At any rate, this data indicates that a longer sequence (i.e., VK13) with valine residues on both termini of the peptide leads to the formation of the most rigid hydrogel. The significantly larger G' observed for VK13 as compared to VK 9 and VK11 may be a result of the formation of a greater number of physical cross-links in its network. This may be due to the increased surface area of the longer peptide, which is available to make more intermolecular contacts as compared to the shorter sequences. Longer sequences greater than 13 residues were not investigated to keep the cost of synthesis as low as possible.

When comparing the gel forming properties of peptides with an odd number of residues as opposed to an even number of residues (e.g., VK9, 11, and 13 versus VK10 and 12), it is apparent that peptides with an even number of residues are unable to form gels of any significant rigidity. Examining the sequence of these peptides shows that those having an even number of residues contain positive point charges at both their N- and C-termini, the N-terminal ammonium of valine and the side-chain ammonium of lysine at the C-terminus (Table 1). Peptides containing an odd number of residues contain only one terminal positive charge from their N-terminal valine ammonium group; their C-terminus is occupied by an amidated valine residue. This observation suggests that N- and C-terminal charges play an important role in self-assembly. In order for VK10 or VK12 to self-assemble, whether it be in an antiparallel or parallel fashion, charge repulsion between the ends of distinct peptides must be overcome. Both the CD and rheology data suggest that, in fact, these repulsions cannot be overcome and inhibit the self-assembly process. Conversely, VK9, 11, and 13 having only the N-terminal charge, can circumvent this potential problem by self-assembling in an antiparallel fashion. This hypothesis was tested by preparing an N-terminally acetylated variant of VK10, namely Ac-VK10. This peptide contains a neutral N-terminus, but still retains its positively charged C-terminal lysine side-chain. Thus, self-assembly in an antiparallel fashion is now a possibility. Both CD and rheology show that this peptide can indeed self-assemble, forming a moderately rigid hydrogel rich in β-sheet secondary structure (see Supporting Information). Further, a study by Nilsson et al. nicely showed that small β-strand amphiphiles acetylated at their N-terminus could self-assemble in an antiparallel fashion upon the addition of various concentrations of salt.[6]

CD spectra were collected for the VK9-13 peptides using solution conditions that should promote gelation. Spectra were obtained for 2 wt% samples of peptide at 35 °C (Figure 3C).

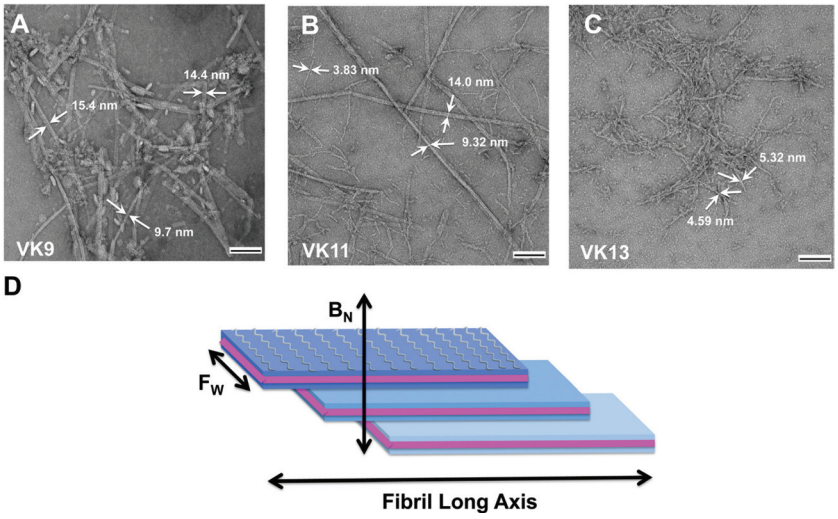

Figure 4. TEM images of VK9, VK11 and VK13 hydrogels depicting the local morphology of fibrils that constitute each gel. Fibrillar structure of VK9 (A), VK11 (B), and VK13 (C) negatively stained with uranyl acetate (scale bar 100 nm). D) Each fibril, which is composed of a bilayer, can undergo lamination to form fibers that are defined morphologically by: F_w, which is defined by the length of each respective β-strand peptide and B_n, the number of stacked bilayers in each laminate. The height of each bilayer in any given fibril is approximately 2.5 nm. F_w(VK9) = 3.0 nm; F_w(VK11) = 3.7 nm; and F_w(VK13) = 4.5 nm. The overall dimensions of fibers are shown in each microscopy image.

Under these experimental conditions all of the odd sequence length peptides accept for VK9 displayed β-sheet structure, evident by the observed minima at 216 nm, while VK10 and VK12 remained random coil. This observation demonstrates that the evolution of β-sheet structure leads to hydrogelation. In addition, it shows that having an N-terminal lysine (e.g., VK10 and VK12) is detrimental to self-assembly leading to gelation. Although no β-sheet structure was observed for VK9 at 2 wt%, the peptide is able to form a gel at a concentration of 4 wt%. Thus, the hydrogelation of VK9 is concentration dependent, unlike the even length peptides, which fail to form a gel even at 4 wt%.

2.4. Local Fibrillar Morphology of VK Peptides

Figure 4 shows transmission electron microscopy (TEM) images, highlighting the local morphology of fibers formed by each peptide, VK9, VK11, and VK13. The microscopy data for all the peptides, taken together, suggests that these molecules self-assemble in a hierarchal fashion.[17] Peptides adopt β-strand conformation as they hydrogen bond to each other forming extended β-sheets. Each β-sheet contains a hydrophobic and hydrophilic face. The aqueous solution drives the association of the hydrophobic faces of two sheets resulting in bilayer formation and the evolution of a growing fibril. Thus, each fibril is a bilayer of β-sheets and each sheet is composed of intermolecularly H-bonded β-strands along the β-sheet's long axis. In this scenario, the width of a given fibril (F_w) is equal to the length of a respective peptide in the β-strand conformation. Lastly, depending on the exact peptide sequence, fibrils can further associate via lamination, resulting in the formation of mature

fibers. When fibers are introduced to a grid for imaging, they can lay down in one of two manners. They can lay flat with the hydrophilic face of one of their β-sheets contacting the grid. In this case, fiber widths would be defined by the length of their respective peptide, regardless of how extensively fibrils have laminated (Figure 4). However, fibers can also lay down on their side. Here, the width of a given fiber will be defined by the number of bilayers (B_N) that have laminated to form the mature fiber.

For VK9 and VK11, TEM shows that these peptides self-assemble into fibrils that have undergone higher order assembly resulting in laminated fibers. VK9 features fibers that are ≈15 nm in width. If fibers have laid down on their side on the grid and since each bilayer is ≈2.5 nm, this suggests that roughly six individual fibrils have associated to form the mature fiber. Also evident are less mature fibers of smaller width (≈9 nm) (Figure 4A). VK11 assembles into fibers of varying widths. Fibers with five and seven bilayers (e.g., B_N = 5, 7) are evident (Figure 4B). In addition, fibers that have laid down flat are also seen (F_W = β-strand width = 3.8 nm). Lastly, VK13 showed only individual fibrils and no higher order laminates. Each fibril has a width of about 4.5 nm, corresponding to the length of an individual VK13 peptide. TEM also shows that the fibrils formed by all the peptides are not twisted, suggesting that the β-sheets formed during assembly are relatively flat.

Although speculative, a possible correlation between the mechanical rigidity of the gels and the local morphology of their respective assemblies can be made. The single fibrils formed by VK13, as opposed to higher order laminated fibers, afford the most rigid hydrogel. It may be that the smaller-in-width and more flexible single fibrils can entangle more efficiently in the three-dimensional gel network affording more rigid networks.

2.5. Influence of Amino Acid Hydrophobicity and Charge

2.5.1. Rheological Properties of XZ13 Hydrogels

Based on the above studies, VK13 was identified as the peptide with the ideal length, whose self-assembly leads to the most rigid hydrogel. Using VK13 as a basis peptide, its hydrophobic content was varied in an effort to fine-tune the material properties of this 13 amino acid peptide sequence. To investigate the effects of altering the hydrophobic content of the peptide, all the valines within the VK13 peptide were replaced with either alanine, leucine or isoleucine residues, while leaving the lysine residues unchanged. These modifications yielded the peptides AK13, LK13, and IK13. An additional peptide, VR13, was prepared to study the role of the lysine residues in providing the positive charge to the peptide. In VR13, all of the lysine residues of VK13 were globally replaced with arginines (Table 1). All of these peptides are collectively referred to as the XZ13 peptides.

Hydrogels were prepared at a concentration of 1 wt% and their viscoelastic properties studied by oscillatory rheology. **Figure 5**A shows dynamic time sweep (DTS) data for all XZ13 peptide gels. The rate of hydrogel formation and overall mechanical rigidity varied significantly between the peptide gels, demonstrating that the amino acid content on the

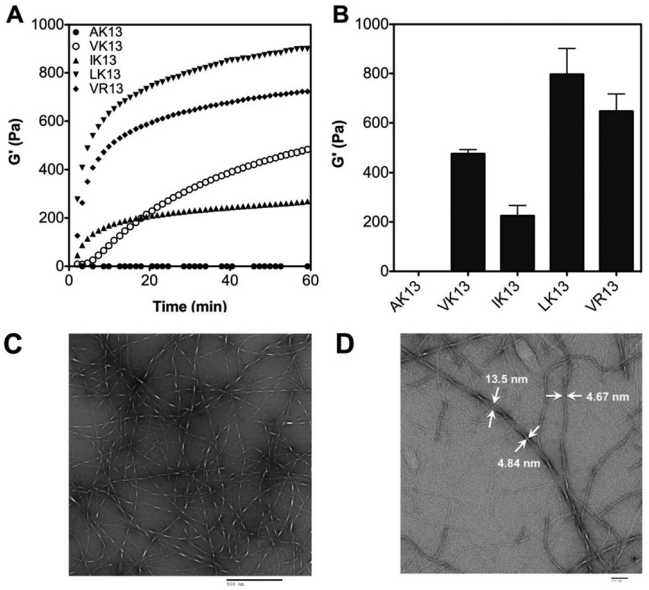

Figure 5. Oscillatory rheology of XZ13 hydrogels. A) Time-sweeps of 1 wt% hydrogels. B) Comparison of storage moduli of hydrogels 1 h post initiating gelation. C,D) TEM microscopy images of LK13 fibers. Scale bars = 500 and 150 nm, respectively.

peptide's hydrophobic face is important in defining gelation. Increasing the hydrophobicity by replacing valine with leucine leads to a more rigid gel. Of the gels studied, LK13 formed the most rigid hydrogel (G' of 795 ± 105 Pa) and displayed fast gelation kinetics (Figure 5B). Conversely, decreasing the hydrophobic surface area of the peptide, as in AK13, results in the inability of the peptide to form a hydrogel. Interestingly, IK13, which has an identical hydrophobic content as compared to LK13,[18] formed a significantly weaker gel. This observation suggests that hydrophobic content, although important, is not the only factor contributing to self-assembly. The exact identity of the hydrophobic side chain is critical in defining its ability to pack efficiently in the self-assembled state.[19] For these linear sequences, leucine may pack more efficiently than isoleucine in the hydrophobic interior of a given fibril.

The identity of the amino acid bearing the positive charge (K versus R) clearly effects the overall bulk material properties of these peptide gels. A faster forming, more rigid gel was obtained through the global replacement of lysine with arginine (VR13). VR13 had the second fastest gelation kinetics and overall rigidity with a final G' of 648 ± 70 Pa. The improved material properties of VR13 versus VK13 could be the result of like-charge pairing of the guanidinium side chains in the aqueous environment of the gel. Although counterintuitive, charged arginine side chains that are solvated can interact favorably via bridging water molecules.[20]

For a hydrogel construct to be delivered via syringe, the gel must exhibit shear-thin recovery behavior. Therefore, the ability of all XZ13 peptides to shear-thin and self-heal was determined by oscillatory rheology. In this experiment, gels were allowed to cure on the rheometer for 60 min before the application of 1000% strain. This amount of strain converts these moderately rigid gels to gels that flow. After 30 s, the strain is decreased

to 0.2% and the gel is allowed to recover for an additional 60 min. Immediate recovery was observed for all peptides (Figure S22, Supporting Information). The gels also displayed slightly faster recovery rates as compared to the initial rates of gelation. The faster recovery kinetics suggests that not all of the crosslinks in the network are disrupted during shear-thinning and those that are disrupted can easily recover.

Although the inclusion of arginine in the primary sequence resulted in stiffer gels, the ability of the VR13 gel to recover after shear-thinning was inconsistent. Different samples of peptide displayed exceedingly different recovery properties. Because we were unable to determine the underlying cause for this behavior, we decided to limit future studies to only the lysine-containing sequences. Thus, the data taken together indicate that LK13 is the optimal sequence, forming the most rigid gel capable of reproducible shear thin-recovery behavior. This behavior allows these gels to be delivered from a simple syringe.

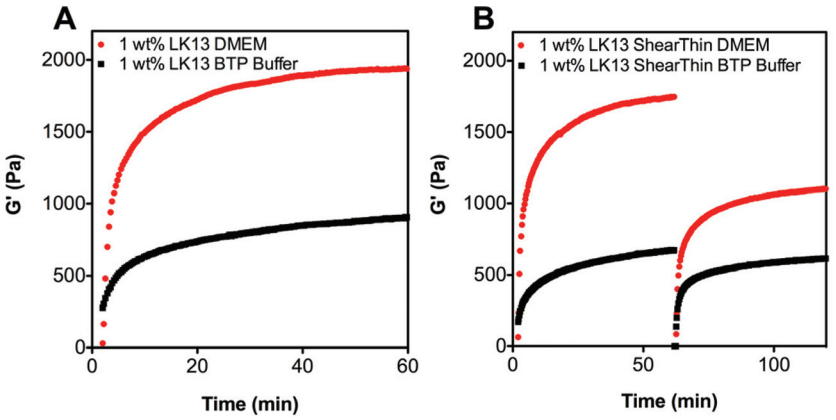

Figure 6. Hydrogelation and shear-thinning/self-healing properties of LK13 in cell culture media vs. BTP buffer. A) Time-sweep measurements of 1 wt% LK13 peptide hydrogel after the addition of either 100 mM BTP and 300 mM NaCl pH 7.4 (■) or DMEM media (●) to an aqueous solution of each peptide. B) Shear thin and self-healing properties of 1 wt% LK13 hydrogel was assessed by monitoring G' as a function of time after shear-thinning of the gel prepared with either DMEM media (●) or 100 mM BTP and 300 mM NaCl buffer (■). The left half of the graph represents the onset of gelation for the initial gelation event at 0.2% strain. The right half of the graph represents shear-thinning at 1000% strain and the immediate recovery of all hydrogels on removing the strain to 0.2%. Frequency = 6 rad s^{-1} for all measurements.

2.5.2. Local Morphology of LK13 Fibrils

High-resolution TEM shows that LK13 forms fibers having a distinct morphology as compared to the valine-containing fibrils. Most apparent is a regular twist, which is the result of the intertwining of individual fibrils around a common screw axis (Figure 5C). Individual fibrils can be seen in the magnified image (Figure 5D) coming together to form the twisted fibers. The thin, bright areas along a twisted fiber measures ≈4.8 nm and corresponds to the length of one LK13 peptide. This indicates that in this area of the laminated fibril, it is laying down flat with one of its β-sheets contacting the grid. The dark areas along a twisted fiber measure 13.5 nm and correspond to about five bilayers (B_N = 5) laying on edge. Referring to Figure 4D, although only three bilayers are shown, a slight twist of the laminates shown would result in the twisted fibers observed in Figure 5C,D.

2.6. Cytocompatibility of the LK13 Hydrogel

2.6.1. Cell Culture Induced Gelation

LK13 gels were prepared for cytocompatibility studies employing Dulbecco's modified Eagle's medium (DMEM) cell culture media to initiate gelation. The physiological pH of 7.4 and high salt content (≈165 mM) of the media make it a suitable candidate to trigger self-assembly. **Figure 6**A shows dynamic time sweep data of a 1 wt% LK13 hydrogel prepared either via the addition of BTP saline buffer or serum-free DMEM to an aqueous solution of peptide. Using the optimized LK13 sequence, only 1 wt% of peptide is needed to form moderately rigid gels. Interestingly, the data indicates an approximate two-fold increase in the overall hydrogel rigidity when using DMEM as compared to buffered saline. The observed increase in rigidity is most likely a result of the additional salts in cell culture media that are better able to screen the peptide's charge and drive the formation of hydrophobic interactions. Additional shear-thinning studies reveal that the LK13 peptide prepared with BTP buffer recovers nearly quantitatively, while LK13 prepared with DMEM recovers to only ≈65% of its original rigidity (Figure 6B). The reason for a less than 100% recovery when using DMEM may also be an effect of the additional additives within the cell culture media, hindering the proper reorganization of the peptide network. Although the DMEM-gel is quantitatively less efficient in recovering on the rheometer, it is capable of being efficiently delivered from a syringe.

2.6.2. Live/Dead Studies

The cytocompatibility of a 1 wt% LK13 hydrogel was determined by studying the cytotoxic effects of the gel toward murine C3H10t1/2 mesenchymal stem cells. Two-dimensional proliferation of cells on the surface of the gel was first assessed through the use of a live/dead cell viability assay. Cells were introduced to the surface of the gel and allowed to incubate for 2 days. **Figure 7**A,B illustrates very good overall cell viability on the surface of the gel, with live cells fluorescing green and dead cells fluorescing red. The LK13 gel shows only a very slight observable decrease in viability as compared to the tissue culture treated polystyrene (TCTP) control surface. Next, cells were directly encapsulated within the three-dimensional network of the gel. Here, cells suspended in DMEM were directly added to a solution of unfolded peptide. The DMEM initiates gelation directly in the presence of the cells. Figure 7C shows a Z-stack laser scanning confocal microscope (LSCM) image perpendicular to the Z-axis of the gel after a 3 h incubation time. As described above, cell viability was assessed using a live/dead assay. The image shows a homogeneous distribution of cells within the

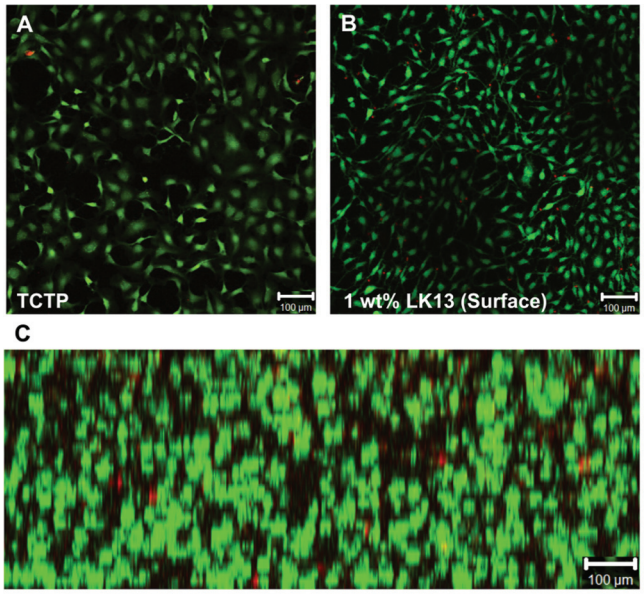

Figure 7. Cytocompatibility studies of the LK13 hydrogel. A,B) Live/dead viability assay performed with murine C3H10t1/2 mesenchymal stem cells incubated for 2 d on the surface of A) TCTP (control) or B) 1 wt% LK13 hydrogel. C) Three-dimensional encapsulation of C3H10t1/2 cells in 1 wt% LK13 hydrogel. Depicted is a LSCM *Z* -stack image (viewed perpendicular to the *Z* -axis) illustrating homogeneous incorporation of cells and cell viability by a live/dead assay 3 h post encapsulation. Viable cells are stained with calcein acetoxymethyl (AM) (green); dead cells are labeled with ethidium homodimer (red). Scale bar = 100 µm.

gel. This suggests that gelation occurs fast enough to trap cells evenly throughout the gel before the cells have a chance to sediment to the bottom of the plate. Importantly, only a very small percentage of cells were compromised during the encapsulation process. The data, taken together, suggest that the LK13 gel is a feasible candidate for cell encapsulation and delivery.

3. Conclusion

An evolution-based design strategy was used to develop a peptide-based hydrogel capable of shear-thin delivery from a simple syringe. This peptide was developed by studying the length and sequence-dependent self-assembly behavior of a small library of short, linear peptides. The optimized peptide, LK13 undergoes saline-triggered self-assembly, forming a network of β-sheet fibrils that define a moderately rigid (G'=797 ± 105 at 1 wt%), self-supporting hydrogel. Cytocompatible LK13 hydrogels can be prepared using cell culture media as the triggering solution, allowing the direct encapsulation of cells in three-dimensions. LK13 gels should find utility in the direct encapsulation and delivery of cells for tissue regenerative therapy.

4. Experimental Section

General Methods and Materials: Trifluoroacetic acid (TFA), piperidine, thioanisole, ethanedithiol, and anisole were purchased from Aldrich. Appropriately side-chain-protected Fmoc-amino acids and 1H-benzotriazolium 1-[bis(dimethylamino)methylene]-5-chloro-hexafluorophosphate(1-)3-oxide (HCTU) were purchased from Novabiochem. C3H10t1/2 cells were obtained from the American Type Culture Collection (ATCC). Dulbecco's modified Eagle medium (DMEM), L-glutamine, gentamicin, sodium chloride, 4-(2-hydroxyethyl)-1-piperazineethanesulfonic acid (HEPES), and bis-trispropane (BTP) were purchased from Sigma. Bovine serum albumin (BSA), trypsin, and phosphate buffer saline (PBS) were obtained from HyClone. The live/dead assay kit was purchased from Invitrogen. Eight-well LabTek confocal dishes were purchased from VWR.

Peptide Synthesis: Peptides were prepared on Pal amide resin via automated Fmoc peptide synthesis employing an ABI 433A or Tribute peptide synthesizer and HCTU activation. The resulting dry resin-bound peptides were cleaved and side-chain-deprotected by use of a trifluoroacetic acid (TFA)/thioanisole/ethanedithiol/anisole (90/5/3/2) cleavage cocktail. Crude peptide was purified by reversed phase-high performance liquid chromatography (RP-HPLC) (preparative Vydac C18 peptide/protein column) employing a linear gradient (see Supporting Information), where solvent A was 0.1% TFA in water and solvent B was 90% acetonitrile, 10% water, and 0.1% TFA. All peptides were isolated via lyophilization yielding white powders. VK9 MS (ESI) 1025.5 [(M + H)+, calcd 1025.8]; VK10 MS (ESI) 1153.5 [(M + H)+, calcd 1153.8]; VK11 MS (ESI) 1252.0 [(M + H)+, calcd 1252.9]; VK12 MS (ESI) 1380.0 [(M + H)+, calcd 1381.0]; VK13 MS (ESI) 1479.0 [(M + H)+, calcd 1480.1]; IK13 MS (ESI) 1578.0 [(M + H)+, calcd 1578.2]; LK13 MS (ESI) 1578.0 [(M + H)+, calcd 1578.2]; AK13 MS (ESI) 1283.7 [(M + H)+, calcd 1283.9]; VR13 MS (ESI) 824.5 $(M+2H)^{2+}$ [$(M + 2H)^{2+}$, calcd 825.6]. See Supporting Information for analytical HPLC and MS data for pure peptides.

Circular Dichroism Studies: CD spectra were collected on an AVIV (Model 420) spectropolarimter. 1 wt% (XZ13 peptides) or 4 wt% (VK9-13 peptides) aqueous stock solutions of peptide were prepared and placed on ice to discourage premature peptide self-assembly. For each peptide, equal volumes (100 µL) of the peptide stock solution and bis-trispropane (BTP) (100 mM, pH7.4) and NaCl (300 mM) were first combined in a small class vial and then transferred immediately to a 0.1 mm path length cylindrical spectrophotometry cell. The final concentrations of peptide were either 0.5 wt% (XZ13 peptides) or 2 wt% (VK9-13 peptides), 50 mM BTP, and 150 mM NaCl. In each case, the cell was placed directly into the instrument cell holder pre-equilibrated at 5 °C and the measurement was started. All samples were measured over a temperature range of 5–70 °C in intervals of 5 °C, except for VK11, which was only investigated at 35 °C when dissolved in water alone. Molar concentrations of peptide solutions were determined by weight. Mean residue ellipticity [θ] was calculated from the equation $[\theta] = (\theta_{obs}/10lc)/r$, where θ_{obs} is the measured ellipticity in millidegrees, l is the length of the cell (cm), c is the concentration (molar), and r is the number of residues.

Hydrogel Preparation: Each peptide is first dissolved in ice-cold deionized, Millipore filtered water followed by the addition of an equal amount of ice-cold BTP buffer (pH 7.4, 100 mM) supplemented with NaCl (300 mM) to induce gelation. Uniform gels were prepared as follows: To prepare 400 µL of a 4 wt% hydrogel peptide (16 mg) is first dissolved in water (200 µL) to give a 8 wt% solution of peptide, followed by the addition of a solution containing 100 mM BTP and 300 mM NaCl (pH 7.4) (200 µL) to yield a final 4 wt% hydrogel in 50 mM BTP and 150 mM NaCl. To investigate hydrogelation properties using cell culture media, 400 µL of a 1 wt% gel is prepared by dissolving peptide (4 mg) in aqueous HEPES (25 mM, pH 7.4) buffer (200 µL) followed by the addition of serum-free DMEM culture media. In each case, after very minimal mixing the resulting gel solutions are immediately investigated by CD or rheology.

Rheology: Dynamic frequency, time, and strain sweep rheology experiments were performed on an AR-G2 rheometer by TA instruments with a 25 mm diameter parallel plate geometry and a gap height of 500 nm. All measurements were performed at 37 °C. Gels were prepared as described above and investigated either at a concentration of 1 or 4 wt% for 1 h or 3 h respectively. Gelation was monitored by performing

a dynamic time sweep (DTS) to measure the storage (G') and loss (G'') modulus at a frequency of 6 rad s^{-1} and 0.2% strain as a function of time for either 3 h or 1 h (see above). This measurement was followed by a dynamic frequency sweep (DFS) (0.1-100 rad s^{-1} at constant 0.2% strain) and a dynamic strain sweep (DSS) (0.1-1000% strain at constant 6 rad s^{-1}), which was used to ensure that the former measurements were within the linear viscoelastic regime. Shear thinning and recovery experiments were done by performing a DTS at a frequency of 6 rad s^{-1} and 0.2% strain for 1 h, immediately followed by a 30 s period, in which 1000% strain at a frequency of 6 rad s^{-1} was applied to the sample. These measurements were then followed by an additional 1 h DTS (6 rad s^{-1}, 0.2% strain) to determine the sample's modulus recovery after shear.

Transmission Electron Microscopy: The hydrogel nanostructure of 4 wt% hydrogels was investigated by preparing an 8 wt% peptide stock solution by dissolving 8 mg of peptide in 100 µL of H_2O, followed by the addition of 100 µL BTP buffer (100 mM BTP, 300 mM NaCl, pH 7.4). The solution was mixed and placed in a 37 °C incubator overnight to allow for fibril formation and gelation. The next day, the sample was prepared for TEM analysis by suspending 5 µL of the prepared gel in 195 µL of H_2O to yield a 40× dilution. Small amounts (5 µL) of each diluted hydrogel solution were applied to separate carbon coated copper grids. Excess solution was removed by filter paper after 1 min. The grid was then washed with deionized water. A 1% (w/v) uranyl acetate aqueous solution was placed on each grid for negative staining and excess staining solution was blotted with filter paper and left to air dry. Bright-field images of the samples were taken on a Hitachi H7600 (Tokyo, Japan).

Cell Viability Assays: Stock C3H10t1/2 cells used in this study were cultured in DMEM media supplemented with 25 mM HEPES, 10% fetal bovine serum (FBS), 5 mM L-glutamine, and 50 µg mL^{-1} Gentamicin at 37 °C in 5% CO_2. For cell viability studies on the hydrogel surface a 1 wt% gel was first prepared by adding an equal volume of serum-free DMEM media to a vial containing a solution of buffered peptide in 25 mM HEPES (pH 7.4). The resultant solution was immediately transferred to an eight-well borosilicate confocal plate and placed into an incubator at 37 °C and 5% CO_2 and allowed to cure for 3 h. 200 µL of serum-free DMEM media was added to the top of the gel and the gel was allowed to equilibrate overnight. The next day C3H10t1/2 cells were trypsinized and counted using a hemacytometer. The resulting cell suspension was diluted with serum supplemented DMEM and added to each well of the 8-well LabTek confocal microscope dish. Cells were plated at a density of 20 000 cells cm^{-2} in 400 µL of serum supplemented DMEM media onto the gel surface and the TCTP culture plate as a control. Cells plated onto the control surface and on top of the gel were incubated for 2 d at 37 °C in 5% CO_2. After the incubation period, the media was removed and each well was washed gently with serum-free DMEM media to allow for the removal of serum proteins, as the presence of serum proteins can lead to an increase in background fluorescence. The viability of cells was then assessed through the use of a live/dead assay. To this end, a stock solution containing both 1 µM calcein AM and 2 µM ethidium homodimer in serum-free DMEM media was prepared and added to each well (200 µL per well). The dye was allowed to incubate for 10 min before removal and subsequent confocal imaging. All gel/cell constructs were imaged by using 10× magnification on a 510 LSCM microscope (Zeiss, Jena, Germany).

To assess the viability of cells encapsulated within a 1 wt% gel, the peptide was first dissolved in an aqueous solution of 25 mM HEPES pH 7.4. An equal amount of the peptide solution and a suspension of 2.5×10^6 C3H10t1/2 cells in DMEM (serum-free) media were then combined and mixed by gentle pipetting to allow for homogenous encapsulation, followed by immediate deposit of the gel/cell construct into an 8-well confocal dish (200 µL per well) before complete gelation occurs. The gel/cell construct was placed into an incubator at 37 °C, 5% CO_2 and allowed to cure for 30 min. After 30 min, the surface of the gel was replenished with fresh serum supplemented DMEM (200 µL per well) and incubated for an additional 3 h before live/dead imaging by confocal microscopy. Live/dead assay of encapsulated cells is performed in the same manner as described above. LSCM Z-stack images were obtained to allow for a 3D viewing of the gel/cell construct.

Supporting Information

Supporting Information is available from the Wiley Online Library or from the author.

Acknowledgements

This work was supported by the Intramural Research Program of the National Cancer Institute of the National Institutes of Health. The authors would like to acknowledge Katelyn Nagy and Kunio Nagashima for their work with TEM imaging.

Received: September 29, 2011
Published online: December 8, 2011

[1] a) J. Kopecek, J. Y. Yang, *Polym. Int.* **2007**, *56*, 1078; b) S. Van Vlierberghe, P. Dubruel, E. Schacht, *Biomacromolecules* **2011**, *12*, 1387; c) J. P. Liu, H. Song, L. L. Zhang, H. Y. Xu, X. J. Zhao, *Macromol. Biosci.* **2010**, *10*, 1164.
[2] O. Wichterle, D. Lim, *Nature* **1960**, *185*, 117.
[3] T. R. Hoare, D. S. Kohane, *Polymer* **2008**, *49*, 1993.
[4] a) M. C. Branco, D. M. Sigano, J. P. Schneider, *Curr. Opin. Chem. Biol.* **2011**, *15*, 427; b) H. Cui, E. T. Pashuck, A. Cheetham, W. Tsai, S. Mui, S. Stupp, *Biopolymers* **2009**, *92*, 298; c) J. E. Gough, V. Jayawarna, S. M. Richardson, A. R. Hirst, N. W. Hodson, A. Saiani, R. V. Ulijn, *Acta Biomater.* **2009**, *5*, 934; d) S. Y. Fung, H. Yang, P. T. Bhola, P. Sadatmousavi, E. Muzar, M. Y. Liu, P. Chen, *Adv. Funct. Mater.* **2009**, *19*, 74; e) Y. B. Yu, Y. Feng, M. Lee, M. Taraban, *Chem. Commun.* **2011**, *47*, 10455; f) E. Gazit, A. Mahler, M. Reches, M. Rechter, S. Cohen, *Adv. Mater.* **2006**, *18*, 1365; g) E. Ingham, S. Maude, D. E. Miles, S. H. Felton, J. Ingram, L. M. Carrick, R. K. Wilcox, A. Aggeli, *Soft Matter* **2011**, *7*, 8085; h) F. Gelain, L. D. Unsworth, S. G. Zhang, *J. Controlled Release* **2010**, *145*, 231; i) D. N. Woolfson, *Biopolymers* **2010**, *94*, 118; j) J. H. Collier, J. P. Jung, J. Z. Gasiorowski, *Biopolymers* **2010**, *94*, 49; k) B. Xu, Y. Gao, Z. M. Yang, Y. Kuang, M. L. Ma, J. Y. Li, F. Zhao, *Biopolymers* **2010**, *94*, 19.
[5] a) J. P. Schneider, D. J. Pochan, B. Ozbas, K. Rajagopal, L. Pakstis, J. Kretsinger, *J. Am. Chem. Soc.* **2002**, *124*, 15030; b) R. H. Nagarkar, R. Pochan, D. Schneider, *J. Biopolymers* **2010**, *94*, 141.
[6] C. J. Bowerman, W. Liyanage, A. J. Federation, B. L. Nilsson, *Biomacromolecules* **2011**, *12*, 2735.
[7] J. D. Ding, L. Yu, *Chem. Soc. Rev.* **2008**, *37*, 1473.
[8] J. D. Kretlow, L. Klouda, A. G. Mikos, *Adv. Drug Delivery Rev.* **2007**, *59*, 263.
[9] a) J. H. Collier, P. B. Messersmith, *Adv. Mater.* **2004**, *16*, 907; b) R. M. Capito, H. S. Azevedo, Y. S. Velichko, A. Mata, S. I. Stupp, *Science* **2008**, *319*, 1812; c) M. M. Stevens, H. F. Qanadilo, R. Langer, V. P. Shastri, *Biomaterials* **2004**, *25*, 757; d) B. M. Gillette, J. A. Jensen, B. X. Tang, G. J. Yang, A. Bazargan-Lari, M. Zhong, S. K. Sia, *Nat. Mater.* **2008**, *7*, 636; e) L. Aulisa, H. Dong, J. D. Hartgerink, *Biomacromolecules* **2009**, *10*, 2694; f) H. Yokoi, T. Kinoshita, S. G. Zhang, *Proc. Natl. Acad. Sci. USA* **2005**, *102*, 8414; g) X. Q. Wang, J. A. Kluge, G. G. Leisk, D. L. Kaplan, *Biomaterials* **2008**, *29*, 1054.
[10] a) D. Cohn, A. Sosnik, S. Garty, *Biomacromolecules* **2005**, *6*, 1168; b) M. C. Hacker, L. Klouda, B. B. Ma, J. D. Kretlow, A. G. Mikos, *Biomacromolecules* **2008**, *9*, 1558; c) S. Wang, D. Nagrath, P. C. Chen, F. Berthiaume, M. L. Yarmush, *Tissue Eng.* **2008**; d) K. Nagapudi, W. T. Brinkman, B. S. Thomas, J. O. Park, M. Srinivasarao, E. Wright, V. P. Conticello, E. L. Chaikof, *Biomaterials* **2005**, *26*, 4695; e) W. A. Petka, J. L. Harden, K. P. McGrath, D. Wirtz, D. A. Tirrell, *Science* **1998**, *281*, 389; f) H. Yan, A. Nykanen, J. Ruokolainen,

D. Farrar, J. E. Gough, A. Saiani, A. F. Miller, *Faraday Discuss.* **2008**, *139*, 71; g) L. S. Nair, T. Starnes, J. W. Ko, C. T. Laurencin, *Biomacromolecules* **2007**, *8*, 3779; h) N. Bhattarai, H. R. Ramay, J. Gunn, F. A. Matsen, M. Zhang, *J. Controlled Release* **2005**, *103*, 609; i) E. S. Gil, D. J. Frankowski, R. J. Spontak, S. M. Hudson, *Biomacromolecules* **2005**, *6*, 3079; j) E. Ruel-Gariepy, J. C. Leroux, *Eur. J. Pharm. Biopharm.* **2004**, *58*, 409; k) L. Klouda, A. G. Mikos, *Eur. J. Pharm. Biopharm.* **2008**, *68*, 34.

[11] a) S. Toledano, R. J. Williams, V. Jayawarna, R. V. Ulijn, *J. Am. Chem. Soc.* **2006**, *128*, 1070; b) Z. Yang, M. Ma, B. L. Xu, *Soft Matter* **2009**, *5*, 2546; c) K. A. Mosiewicz, K. Johnsson, M. P. Lutolf, *J. Am. Chem. Soc. 132*, 5972; d) J. H. Collier, P. B. Messersmith, *Bioconjugate Chem.* **2003**, *14*, 748; e) H. W. Jun, V. Yuwono, S. E. Paramonov, J. D. Hartgerink, *Adv. Mater.* **2005**, *17*, 2612.

[12] a) Q. Li, J. Wang, S. Shahani, D. D. Sun, B. Sharma, J. H. Elisseeff, K. W. Leong, *Biomaterials* **2006**, *27*, 1027; b) A. N. Buxton, J. Zhu, R. Marchant, J. L. West, J. U. Yoo, B. Johnstone, *Tissue Eng.* **2007**, *13*, 2549; c) H. A. Declercq, M. J. Cornelissen, T. L. Gorskiy, E. H. Schacht, *J. Mater. Sci. Mater. Med.* **2006**, *17*, 113; d) A. A. Aimetti, A. J. Machen, K. S. Anseth, *Biomaterials* **2009**, *30*, 6048; e) B. D. Polizzotti, B. D. Fairbanks, K. S. Anseth, *Biomacromolecules* **2008**, *9*, 1084; f) B. Sharma, C. G. Williams, M. Khan, P. Manson, J. H. Elisseeff, *Plast. Reconstr. Surg.* **2007**, *119*, 112.

[13] a) C. Q. Yan, A. Altunbas, T. Yucel, R. P. Nagarkar, J. P. Schneider, D. J. Pochan, *Soft Matter* **2010**, *6*, 5143; b) J. P. Schneider, M. C. Branco, D. J. Pochan, N. J. Wagner, *Biomaterials* **2010**, *31*, 9527; c) J. P. Schneider, R. V. Rughani, M. C. Branco, D. Pochan, *Macromolecules* **2010**, *43*, 7924; d) D. Salick, D. Pochan, J. Schneider, *Adv. Mater.* **2009**, *21*, 4120; e) M. C. Branco, D. J. Pochan, N. J. Wagner, J. P. Schneider, *Biomaterials* **2009**, *30*, 1339; f) L. Haines-Butterick, K. Rajagopal, M. Branco, D. Salick, R. Rughani, M. Pilarz, M. S. Lamm, D. J. Pochan, J. P. Schneider, *Proc. Natl. Acad. Sci. USA* **2007**, *104*, 7791.

[14] a) E. L. Bakota, Y. Wang, D. Farhad, J. Hartgerink, *Biomacromolecules* **2011**, *12*, 1651; b) S. Ramachandran, Y. Tseng, Y. B. Yu, *Biomacromolecules* **2005**, *6*, 1316.

[15] A. Brack, L. E. Orgel, *Nature* **1975**, *256*, 383.

[16] J. K. Schneider, *J. Am. Chem. Soc.* **1995**, *117*, 2533.

[17] N. Boden, A. Aggeli, I. A. Nyrkova, M. Bell, R. Harding, L. Carrick, T. C. B. McLeish, A. N. Semenov, *Proc. Natl. Acad. Sci. USA* **2001**, *98*, 11857.

[18] C. P. Moon, K. G. Fleming, *Proc. Natl. Acad. Sci. USA* **2011**, *108*, 10174.

[19] K. Wang, J. D. Keasling, S. J. Muller, *Int. J. Biol. Macromol.* **2005**, *36*, 232.

[20] a) J. Vondrasek, P. E. Mason, J. Heyda, K. D. Collins, P. Jungwirth, *J. Phys. Chem. B* **2009**, *113*, 9041; b) A. Magalhaes, B. Maigret, J. Hoflack, J. N. Gomes, H. A. Scheraga, *J. Protein Chem.* **1994**, *13*, 195.